

Constraining Parameters of Generalized Cosmic Chaplygin Gas in Loop Quantum Cosmology

Chayan Ranjit¹

Ujjal Debnath²

February 25, 2018

Received _____; accepted _____

arXiv:1409.7057v1 [physics.gen-ph] 20 Sep 2014

¹Department of Mathematics, Seacom Engineering College, Howrah - 711 302, India. Email: chayanranjit@gmail.com

²Department of Mathematics, Indian Institute of Engineering Science and Technology, Shibpur, Howrah-711 103, India. Email: ujjaldebnath@yahoo.com

ABSTRACT

We have assumed the FRW universe in loop quantum cosmology (LQC) model filled with the dark matter and the Generalized Cosmic Chaplygin gas (GCCG) type dark energy where dark matter follows the linear equation of state. We present the Hubble parameter in terms of the observable parameters Ω_{m0} and H_0 with the redshift z and the other parameters like A , B , w_m , ω and α which coming from our model. From Stern data set (12 points)& SNe Type Ia 292 data (from Riess et al. (2004, 2007); Astier et al. (2006)) we have obtained the bounds of the arbitrary parameters by minimizing the χ^2 test. The best-fit values of the parameters are obtained by 66%, 90% and 99% confidence levels. Next due to joint analysis with Stern+BAO and Stern+BAO+CMB observations, we have also obtained the bounds of the parameters (A, B) by fixing some other parameters α , w_m and ω . From the best fit values of the parameters, we have obtained the distance modulus $\mu(z)$ for our theoretical GCCG model in LQC and from Supernovae Type Ia (union2 sample 552 data from [Amanullah et al. (2010)] & Riess 292 data from [Riess et al. (2004, 2007); Astier et al. (2006)]), we have concluded that our model is in agreement with the Supernovae Type Ia sample data. In addition, we have investigated in details about the various types of Future Singularities that may be formed in this model and it is notable that our model is completely free from any types of future singularities.

1. Introduction

It is known from recent observational study that our universe is expanding with an acceleration and that supported by different observations of the SNeIa [Perlmutter et al. (1998, 1999); Riess et al. (1998, 2004)], baryon acoustic oscillations (BAO) [Eisenstein et al. (2005)], large scale redshift surveys [Bachall et al. (1999); Tedmark et al. (2004)], the measurements of the cosmic microwave background (CMB) [Miller et al. (1999); Bennet et al. (2000)], WMAP

[Bridle et al. (2003); Spergel et al. (2003, 2007)] and effects of weak lensing [Jain et al. (2003)]. The recent trend among the researchers is that to find the methodology that triggers late inflation and for that researchers are mainly divided into two groups, one considering a modification in the geometry by adjusting the form of original general theory of relativity and other invoking any mysterious fluid in the form of an evolving cosmological constant or a quintessential [Peebles et al. (1988)] type of scalar field. Those unknown mysterious fluid which has the property that the positive energy density and sufficient negative pressure, known as dark energy (DE) [Padmanabhan (2003); Sahni et al. (2000)] in which the potential dominates over the kinetic term. In present time, DE related problems are most interesting research topic of theoretical physics [Weinberg (1989)]. There are several interesting form of solution of this type problem such as phantom [Caldwell (2002); Fu et al. (2008)] tachyon scalar field [Sen (2002); Balart et al. (2007); Farajollahi et al. (2011); del Campo et al. (2009)], hessence [Wei et al. (2005)], dilaton scalar field [Morris (2012); Marcus (1990)], K-essence scalar field [Armendariz - Picon et al. (2001); Bouhmadi-Lpez et al. (2010); Malquarti et al. (2003)], DBI essence scalar field [Spalinski (2007); Martin et al. (2008)] and many others.

Another unknown missing matter component of the universe is known as the dark matter (DM) which holds together the galaxy clusters. DM is also needed to explain the current large scale structure of the universe. It can be predicted that in cosmic concordance Λ CDM model, the Universe is formed of 26% matter (baryonic + dark matter) and $\sim 74\%$ of a smooth vacuum energy component, whereas the thermal CMB component contributes only about 0.01%, however, its angular power spectrum of temperature encode important information about the structure formation process and other cosmic observables.

Loop Quantum Gravity (LQG) theory has been basically trying to quantize the gravity with a non-perturbative and background independent way. As a result, the quantum effect of our universe quite comfortably describe by LQG [Ashtekar et al. (2004); Rovelli (1998)]. The theory and principles of LQG when combined with cosmological framework then it creates a new theoretical framework, named as Loop Quantum Cosmology(LQC) [Bojowald (2001, 2002, 2005, 2008); Ashtekar (2007); Ashtekar et al. (2003, 2006, 2008)]. LQC is basically based

on discrete quantum geometry instead of classical space-time continuum. Friedmann equation is modified by adding a term quadratic in density to describe the effect of LQG. In LQC, the standard Friedmann equation is modified with the help of the non-perturbative effects which leads to the correction term $\frac{\rho^2}{\rho_c}$ and which leads to the result of mechanically bouncy universe when the matter energy density reaches to the level of Plank density ρ_c . In 2005, Bojowald [Bojowald (2005)] reviewed to give an overview and summary of the current status of the research work on LQC in detail and that review was also modified by Bojowald (2008). A valuable report about the existing state of art on LQC is discussed in Ashtekar et al. (2011). Recently, Sadjadi [Sadjadi (2013)] has been discussed about the related study on LQC like a super acceleration and its possible phase transitions, i.e., the crossing of the phantom divide line $\omega = -1$.

In observational study, the theoretical models and bounds of the parameters are tested by the combinations of different observations astrophysical data repeatedly. The observational facts are not explained properly by standard big bang cosmology with perfect fluid. Even though in Einstein’s gravity, the cosmological constant Λ (which has the equation of state $w_\Lambda = -1$) allows the cosmic acceleration at late times, but till now there is no proof of the origin of Λ and the observational bounds on Λ are incompatible with theoretical predictions in vacuum state.

For flat universe, if we assume the universe is filled with dust-like matter and dark energy, then we need to know Ω_m of the dust-like matter and $H(z)$ to a very high accuracy in order to get a handle on Ω_X or w_X of the dark energy [Choudhury et al. (2007); Padmanabhan et al. (2003)]. From observations, this can be a fairly degeneracy for determining $w_X(z)$. For $z > 0.01$, TONRY data set with the 230 data points [Tonry et al. (2003)] with the 23 points from Barris et al [Barris et al. (2004)] are still valid. For $1 < z < 1.6$, the “gold” sample of Riess et al [Riess et al. (2004)] with 156 data points are valid. In the flat FRW universe, one finds $\Omega_\Lambda + \Omega_m = 1$, which are currently favoured by CMBR data (for recent WMAP results, see [Spergel et al. (2003)]). For the most recent Riess data set gives a best-fit value of Ω_m to be 0.31 ± 0.04 , which matches with the value $\Omega_m = 0.29_{-0.03}^{+0.05}$ obtained by Riess

et al [Riess et al. (1998)]. In comparison, the best-fit Ω_m for flat models was found to be 0.31 ± 0.08 [Choudhury et al. (2007)]. The best-fit constant equation of state parameter w for Union 2 data sample gives $w = -0.997_{-0.054}^{+0.050}(\text{stat})_{-0.082}^{+0.077}(\text{stat+sys together})$ for a flat universe, or $w = -1.038_{-0.059}^{+0.056}(\text{stat})_{-0.097}^{+0.093}(\text{stat+sys together})$ with curvature [Amanullah et al. (2010)]. Now, Chaplygin gas is the more effective candidate of dark energy with equation of state $p = -B/\rho$ [Kamenshchik et al. (2001)] with $B > 0$. It has been generalized to the form $p = -B/\rho^\alpha$ [Gorini et al. (2003)] and thereafter modified to the form $p = A\rho - B/\rho^\alpha$ [Debnath et al. (2004)]. The MCG best fits with the 3 year WMAP and the SDSS data with the choice of parameters $A = 0.085$ and $\alpha = 1.724$ [Lu et al. (2008)] which are improved constraints than the previous ones $-0.35 < A < 0.025$ [Dao-Jun et al. (2005)].

In this work, we assume the FRW universe in Loop Quantum Cosmology (LQC) model filled with the dark matter and the MCG type dark energy. We present the Hubble parameter in terms of the observable parameters Ω_{m0} and H_0 with the redshift z and the other parameters like A , B , w_m , ω and α in Section 3. From Stern data set (12 points), we obtain the bounds of the arbitrary parameters by minimizing the χ^2 test in Subsection 3.1. The best-fit values of the parameters are obtained by 66%, 90% and 99% confidence levels. Next due to joint analysis with BAO and CMB observations, we also obtain the bounds and the best fit values of the parameters (A, B) by fixing some other parameters $H_0, \Omega_{m0}, w_m, \omega$ and α at their most suitable values in Subsection 3.2 and Subsection 3.3 respectively. From the best fit of distance modulus $\mu(z)$ for our theoretical MCG model in LQC with SNe Type Ia union2 sample 552 data from [Amanullah et al. (2010)] in Subsection 3.4, we conclude that our model is in agreement with the union2 sample data. After that in section 4 we consider the SNe Type Ia Riess 292 data from [Riess et al. (2004, 2007); Astier et al. (2006)] and examine the bounds of the arbitrary parameters A & B by minimizing the χ^2 test for 66%, 90% and 99% confidence levels by fixing $H_0, \Omega_{m0}, w_m, \omega$ and α at their most suitable values and then we draw the distance modulus $\mu(z)$ for our theoretical MCG model in LQC with SNe Type Ia Riess 292 data from [Riess et al. (2004, 2007); Astier et al. (2006)] in Subsection 4.1 and also concluded that our model is in agreement with the Riess 292 sample data. The different types

of singularities of this scenario have been studied in Section 5 and finally, the concluding remarks of the paper are summarized in Section 6.

2. BASIC EQUATIONS AND SOLUTIONS FOR GCCG IN LQC

In recent years, loop quantum gravity (LQG) is outstanding effort to describe the quantum effect of our universe. Nowadays several dark energy models are studied in the framework of LQC. Till now, Quintessence and phantom dark energy models [Wu et al. (2008); Chen et al. (2008)] have been studied in the cosmological evolution in LQC. Then Modified Chaplyng Gas coupled to dark matter in the universe and it was described in the frame work LQC by Jamil et al [Jamil et al. (2011)] who resolved the famous cosmic coincidence problem in modern cosmology. Some authors have studied the model with an interacting phantom scalar field with an exponential potential and deduced that the dark energy dominated future singularities have been appearing in the standard FRW cosmology but some of these singularities may be avoided by loop quantum effects.

We consider the flat homogeneous and isotropic universe described by FRW metric, so the modified Einstein's field equations in LQC are given by [Jamil et al. (2011)]

$$H^2 = \frac{\rho}{3} \left(1 - \frac{\rho}{\rho_c} \right) \quad (1)$$

and

$$\dot{H} = -\frac{1}{2}(\rho + p) \left(1 - \frac{2\rho}{\rho_c} \right) \quad (2)$$

where H is the Hubble parameter defined as $H = \frac{\dot{a}}{a}$ with a is the scale factor. Where $\rho_c = \sqrt{3}\pi^2\gamma^3 G^2 \hbar$ is called the critical loop quantum density, γ is the dimensionless Barbero-Immirzi parameter. Here the universe begins to bounce and then oscillate forever when the energy density of the universe becomes of the same order of the critical density ρ_c . Thus the big bang, big rip and other singularities problems, which could not explained by the Einstein's cosmology, might solve in LQC. It is to be noted that the parameter γ is fixed in LQC by the requirement of the validity of Bekenstein-Hawking entropy for the Schwarzschild black hole and it has been suggested that $\gamma \sim 0.2375$ by the black hole thermodynamics in LQC. The

physical solutions are allowed only when $\rho \leq \rho_c$. For $\rho = \rho_c$, it is called bounce. The maximum value of the Hubble factor H is settled for $\rho_{max} = \frac{\rho_c}{2}$ and the maximum value of Hubble factor is $\frac{\kappa\rho_c}{12}$.

Here $\rho = \rho_x + \rho_m$ and $p = p_x + p_m$, where ρ_m, p_m are the matter-density and pressure contribution of matter respectively and ρ_x, p_x are respectively the energy density and pressure contribution of some dark energy. Now we consider the Universe is filled with Generalized Cosmic Chaplygin Gas (GCCG) model whose equation of state (EOS) is given by [Gonzalez-Diaz (2003); Chakraborty et al. (2007)]

$$p_x = -\rho_x^{-\alpha}[C + (\rho_x^{1+\alpha} - C)^{-\omega}] \quad (3)$$

where $C = \frac{A}{1+\omega} - 1$ with A is a constant which can take on both positive and negative values and $-l < \omega < 0$, l being a positive definite constant which can take on values larger than unity. We also consider the dark matter and the dark energy are separately conserved and the conservation equations of dark matter and dark energy (GCCG) are given by

$$\dot{\rho}_m + 3H(\rho_m + p_m) = 0 \quad (4)$$

and

$$\dot{\rho}_x + 3H(\rho_x + p_x) = 0 \quad (5)$$

From first conservation equation (4) we have the solution of ρ_m as

$$\rho_m = \rho_{m0}(1+z)^{3(1+w_m)} \quad (6)$$

where $p_m = \rho_m w_m$. From the conservation equation (5) we have the solution of the energy density as

$$\rho_x = \left[\left(\frac{A}{1+\omega} - 1 \right) + (1 + B(1+z)^{3(1+\alpha)(1+\omega)})^{\frac{1}{1+\omega}} \right]^{\frac{1}{1+\alpha}} \quad (7)$$

where B is the integrating constant, $z = \frac{1}{a} - 1$ is the cosmological redshift (choosing $a_0 = 1$) and the first constant term can be interpreted as the contribution of dark energy.

3. Observational Data Analysis

From the solution (7) of GCCG and defining the dimensionless density parameter $\Omega_{m0} = \frac{\rho_{m0}}{3H_0^2}$, we have the expression for Hubble parameter H in terms of redshift parameter z as follows ($8\pi G = c = 1$)

$$H(z) = \frac{1}{\sqrt{3}} \left[3\Omega_{m0}H_0^2(1+z)^{3(1+w_m)} + \left(\left(\frac{A}{1+\omega} - 1 \right) (1+B(1+z)^{3(1+\alpha)(1+\omega)})^{\frac{1}{1+\omega}} \right) \right]^{\frac{1}{2}} \\ \times \left[1 - \frac{3\Omega_{m0}H_0^2(1+z)^{3(1+w_m)} + \left(\left(\frac{A}{1+\omega} - 1 \right) (1+B(1+z)^{3(1+\alpha)(1+\omega)})^{\frac{1}{1+\omega}} \right)}{\rho_c} \right]^{\frac{1}{2}} \quad (8)$$

From equation (8), we see that the value of H depends on $H_0, A, B, \Omega_{m0}, w_m, \omega, \alpha, z$. The $E(z)$ can be written as

$$E(z) = \frac{H(z)}{H_0} \quad (9)$$

Now $E(z)$ contains unknown parameters like A, B, ω and α . Now we will fixing two parameters and by observational data set the relation between the other two parameters will obtain and find the bounds of the parameters.

z	$H(z)$	$\sigma(z)$
0	73	± 8
0.1	69	± 12
0.17	83	± 8
0.27	77	± 14
0.4	95	± 17.4
0.48	90	± 60
0.88	97	± 40.4
0.9	117	± 23
1.3	168	± 17.4
1.43	177	± 18.2
1.53	140	± 14
1.75	202	± 40.4

Table 1: The Hubble parameter $H(z)$ and the standard error $\sigma(z)$ for different values of redshift z .

In the following subsections, we shall investigate the data analysis mechanism for Stern, Stern+BAO and Stern+BAO+CMB observational data to find some bound of the parameters of GCCG with LQC. We shall use the χ^2 minimization technique (statistical data analysis) to test the theoretical Hubble parameter with the observed data set to get the best fit values of the unknown parameters with different confidence levels.

3.1. Analysis with Stern ($H(z)$ - z) Data Set

In 2010, Stern et al [Stern et al. (2010)] proposed an observed data set which is known as Stern ($H(z)$ - z) data set. Stern data set consisted with the observed value of Hubble parameter $H(z)$ and the standard error $\sigma(z)$ for different values of redshift z (twelve data points), which are given in Table 1. Here we use Stern data set (twelve data points) to analyze the model. Before going to apply χ^2 minimization technique, we first form the χ^2 statistics as a sum of standard normal distribution as follows:

$$\chi_{Stern}^2 = \sum \frac{(H(z) - H_{obs}(z))^2}{\sigma^2(z)} \quad (10)$$

where $H_{obs}(z)$ and $H(z)$ are observational and theoretical values of Hubble parameter at different redshifts z respectively and $\sigma(z)$ is the corresponding error for the particular observation given in Table 1. Also, the nuisance parameter H_{obs} can be safely marginalized. Here the present value of Hubble parameter H_0 is been settled at $72 \pm 8 \text{ Km s}^{-1} \text{ Mpc}^{-1}$ with a fixed prior distribution. Now we shall determine the bounds of parameters A and B for different α from minimizing the above distribution χ_{Stern}^2 . Fixing the other parameters $\Omega_{m0}, w_m, \omega, \alpha$, the relation between A and B can be determined by the observational data. The probability distribution function in terms of the parameters $A, B, \Omega_{m0}, w_m, \omega$ and α can be written as

$$L = \int e^{-\frac{1}{2}\chi_{Stern}^2} P(H_0) dH_0 \quad (11)$$

where $P(H_0)$ is the prior distribution function for H_0 .

Now, using χ^2 minimization technique, we plot the graph of the unknown parameters A and B for different α and fixing the other parameters for different confidence levels (like 66%, 90% and 99%). The best fit values of the parameters A and B are written in Table 2. It is to be noted that our best fit analysis with Stern observational data support the theoretical range of the parameters.

The 66% (solid, blue), 90% (dashed, red) and 99% (dashed, black) contours for (A, B) are plotted in figures 1, 2 and 3 for different values of α . Also the best fit values of A and B are tabulated in Table 2.

α	A	B	χ^2_{min}
0.0020	0.628976	5.62894	7.09652
0.0010	0.628989	5.62894	7.09652
0.0005	-0.069897	5.58487	7.09670

Table 2: $H(z)$ - z (Stern): The best fit values of A , B and the minimum values of χ^2 for different values of α and fixed value of other parameters.

3.2. Joint Analysis with Stern + BAO Data Sets

Now we use the statistical approach of joint analysis put forwarded by Eisenstein et al Eisenstein et al. (2005). The Baryon Acoustic Oscillation (BAO) peak parameter value has been proposed in their method of joint analysis. Sloan Digital Sky Survey (SDSS) survey is one of the primordial redshift survey by which the BAO signal has been directly detected at a scale ~ 100 Mpc. In this case, the said analysis is actually the combination of angular diameter distance and Hubble parameter at that redshift. This analysis is independent of the measurement of H_0 and not containing any particular dark energy. Here we shall check the parameters A and B with the measurements of the BAO peak at low redshift (with range $0 < z < 0.35$) using standard χ^2 technique. The error, corresponding to the standard deviation, is follow the Gaussian distribution. Low-redshift distance have the ability to measure the Hubble constant H_0 directly. It lightly depends on different cosmological parameters and the

equation of state of dark energy. The BAO peak parameter might be defined as

$$\mathcal{A} = \frac{\sqrt{\Omega_m}}{E(z_1)^{1/3}} \left(\frac{1}{z_1} \int_0^{z_1} \frac{dz}{E(z)} \right)^{2/3} \quad (12)$$

Here $E(z) = H(z)/H_0$ is the normalized Hubble parameter. The redshift z_1 is the typical redshift of the SDSS sample whose value is settled as 0.35 and the integration term is the dimensionless comoving distance to the redshift z_1 . The value of the parameter \mathcal{A} for the flat model of the universe is proposed as Eisenstein et al. (2005) $\mathcal{A} = 0.469 \pm 0.017$ using SDSS data from luminous red galaxies survey. Now the χ^2 function for the BAO measurement can be written as

$$\chi_{BAO}^2 = \frac{(\mathcal{A} - 0.469)^2}{(0.017)^2} \quad (13)$$

Now the total joint data analysis (Stern+BAO) for the χ^2 function is defined by Wu et al. (2007); Thakur et al. (2009); Paul et al. (2010, 2011); Ghose et al. (2012); Chakraborty et al. (2012)

$$\chi_{total}^2 = \chi_{Stern}^2 + \chi_{BAO}^2 \quad (14)$$

According to our analysis the joint scheme gives the best fit values of A and B for different α in Table 3. Finally we draw the contours A vs B for the 66% (solid, blue), 90% (dashed, red) and 99% (dashed, black) confidence limits depicted in figures 4 – 6 for different values of α .

α	A	B	χ_{min}^2
0.0020	1.4401851	5.71536	768.073
0.0010	0.0296015	5.62625	768.073
0.0005	-0.666052	5.58219	768.074

Table 3: $H(z)$ - z (Stern) + BAO : The best fit values of A , B and the minimum values of χ^2 for different values of α and fixed value of other parameters.

3.3. Joint Analysis with Stern + BAO + CMB Data Sets

In this subsection, we shall follow the pathway, proposed by some author [Bond et al. (1997); Efstathiou et al. (1999); Nessaeris et al. (2007)], using Cosmic Microwave Background

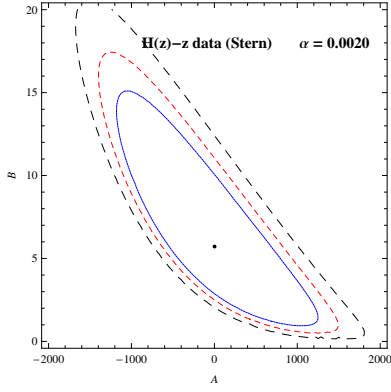


Fig.1

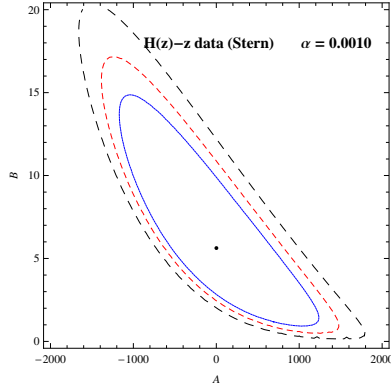


Fig.2

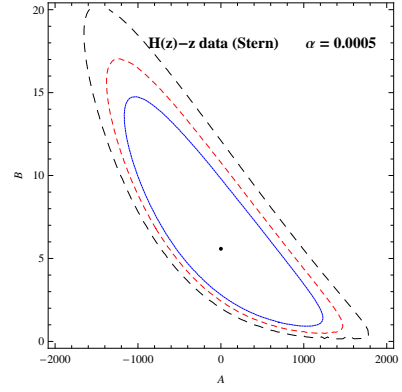


Fig.3

Fig.1-3 show that the variation of A with B for $\Omega_{m0} = 0.0643, w_m = 0.051, \omega = -0.92$ with $\alpha = 0.0020, 0.0010$ & 0.0005 respectively for different confidence levels. The 66% (solid, blue), 90% (dashed, red) and 99% (dashed, black) contours are plotted in these figures for the $H(z)$ - z (Stern) analysis.

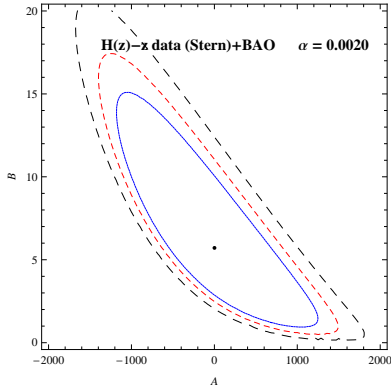


Fig.4

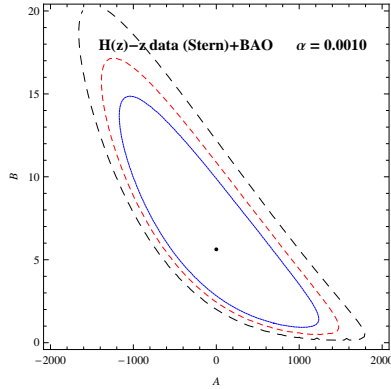


Fig.5

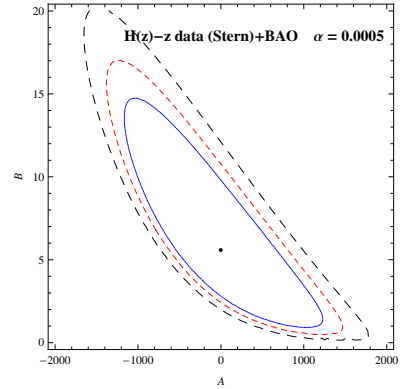


Fig.6

Fig.4-6 show that the variation of A with B for $\Omega_{m0} = 0.01, w_m = 0.051, \omega = -0.92$ with $\alpha = 0.0020, 0.0010$ & 0.0005 respectively for different confidence levels. The 66% (solid, blue), 90% (dashed, red) and 99% (dashed, black) contours are plotted in these figures for the $H(z)$ - z (Stern)+BAO joint analysis.

(CMB) shift parameter. The interesting geometrical probe of dark energy can be determined by the angular scale of the first acoustic peak through angular scale of the sound horizon at the surface of last scattering which is encoded in the CMB power spectrum. It is not sensitive with respect to perturbations but are suitable to constrain model parameter. The CMB power spectrum first peak is the shift parameter which is given by

$$\mathcal{R} = \sqrt{\Omega_m} \int_0^{z_2} \frac{dz}{E(z)} \quad (15)$$

where z_2 is the value of redshift at the last scattering surface.

From WMAP7 data of the work of Komatsu et al Komatsu et al. (2011) the value of the parameter has proposed as $\mathcal{R} = 1.726 \pm 0.018$ at the redshift $z = 1091.3$. Therefore the χ^2 function for the CMB measurement can be written as

$$\chi_{CMB}^2 = \frac{(\mathcal{R} - 1.726)^2}{(0.018)^2} \quad (16)$$

Now when we consider three cosmological tests together, the total joint data analysis (Stern+BAO+CMB) for the χ^2 function may be defined by

$$\chi_{TOTAL}^2 = \chi_{Stern}^2 + \chi_{BAO}^2 + \chi_{CMB}^2 \quad (17)$$

Now the best fit values of A and B for joint analysis of BAO and CMB with Stern observational data support the theoretical range of the parameters given in Table 4. The 66% (solid, blue), 90% (dashed, red) and 99% (dashed, black) contours are plotted in figures 7-9 for different values of α .

α	A	B	χ_{min}^2
0.0020	1.4816294	5.71517	9962.75
0.0010	0.0713549	5.62606	9962.75
0.0005	-0.624274	5.58201	9962.75

Table 4: $H(z)$ - z (Stern) + BAO + CMB : The best fit values of A , B and the minimum values of χ^2 for different values of α and fixed value of other parameters.

3.4. Redshift-Magnitude Observations of Supernovae Type Ia Union2 552

Sample [From Amanullah et al. (2010)]

The main evidence for the existence of dark energy is provided by the Supernova Type Ia experiments. Two teams of High- z Supernova Search and the Supernova Cosmology Project have discovered several type Ia supernovas at the high redshifts [Perlmutter et al. (1998, 1999); Riess et al. (1998, 2004)] since 1995. The observations directly measure the distance modulus of a Supernovae and its redshift z [Riess et al. (2007); Kowalaski et al. (2008)]. Here we take recent observational data, including SNe Ia which consists of 557 data points and belongs to the Union2 sample [Amanullah et al. (2010)].

Motivated by the work of some authors [Thakur et al. (2009); Paul et al. (2010, 2011); Ghose et al. (2012); Chakraborty et al. (2012)] here we determine distance modulus $d_L(z)$ for our theoretical GCCG in LQC model and tested with the SNe Type Ia data. From the observations, the luminosity distance $d_L(z)$ determines the dark energy density and is defined by

$$d_L(z) = (1+z)H_0 \int_0^z \frac{dz'}{H(z')} \quad (18)$$

and the distance modulus (distance between absolute and apparent luminosity of a distance object) for Supernovas is given by

$$\mu(z) = 5 \log_{10} \left[\frac{d_L(z)/H_0}{1 \text{ Mpc}} \right] + 25 \quad (19)$$

The best fit of distance modulus as a function $\mu(z)$ of redshift z for our theoretical model and the Supernova Type Ia Union2 sample are drawn in figure 10 for our best fit values of A , B with the other previously chosen parameters. In Figure 11, we have shown that the variation of the curves with slightly changes in the value of A and B ($A = 0.001$ & $B = 0.13$ for Black line; $A = 0.03$ & $B = 0.05$ for Red line; $A = 0.002$ & $B = 0.025$ for Green line). From the curves, we see that the theoretical GCCG with LQC is in agreement with the union2 sample data.

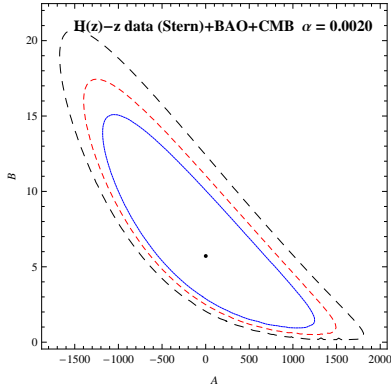


Fig.7

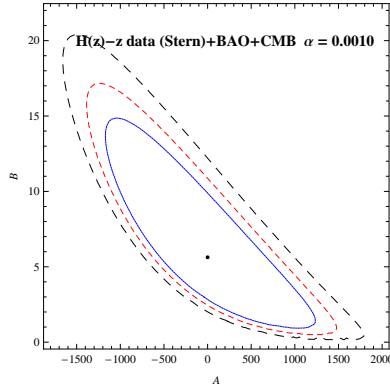


Fig.8

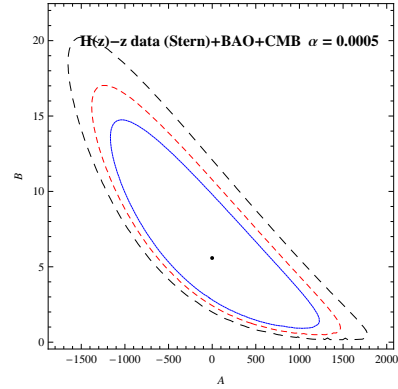


Fig.9

Fig.7-9 show that the variation of A with B for $\Omega_{m0} = 0.01, w_m = 0.051, \omega = -0.92$ with $\alpha = 0.0020, 0.0010$ & 0.0005 respectively for different confidence levels. The 66% (solid, blue), 90% (dashed, red) and 99% (dashed, black) contours are plotted in these figures for the $H(z)$ - z (Stern)+BAO+CMB analysis.

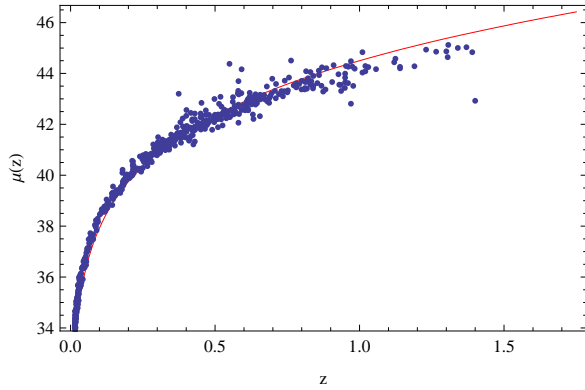


Fig.10

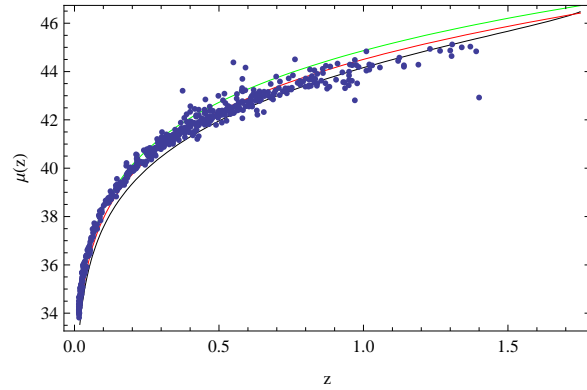


Fig.11

Fig.10 show $\mu(z)$ vs z for our GCCG with LQC (solid red line) and the Union2 sample (dotted points). Fig 11 shows the same for different value of A & B ($A = 0.001$ & $B = 0.13$ for Black line; $A = 0.03$ & $B = 0.05$ for Red line; $A = 0.002$ & $B = 0.025$ for Green line).

4. Analysis with Supernovae Type Ia 292 Data [From Riess et al. (2004, 2007); Astier et al. (2006)]

In this section we analyzed our GCCG with LQC model with same spirit (as stated before in the previous sections) and obtaining the bounds of the arbitrary parameters (A & B) by fixing the cosmological parameters around their favorable value with the help of observational 292 Supernovae Type Ia data which belongs to [Riess et al. (2004, 2007); Astier et al. (2006)] and also shown in Table 5 at Appendix. As like Sec. 3.1, here also we are applying χ^2 minimization technique, where the χ^2 statistics is as follows:

$$\chi_{(SNeTypeIa)}^2 = \sum \frac{(H(z) - H_{obs}(z))^2}{\sigma^2(z)} \quad (20)$$

where the $H_{obs}(z)$ and $\sigma(z)$ are given in Table 5 and also the probability distribution function can be expressed as

$$L = \int e^{-\frac{1}{2}\chi_{(SNeTypeIa)}^2} P(H_0) dH_0 \quad (21)$$

where $P(H_0)$ is the prior distribution function for H_0 . By using χ^2 minimization technique, here we plot the graph of the unknown parameters A and B for same values of α (as stated above) and fixing the other parameters for their most suitable values and draw for different confidence levels (as 66%, 90% and 99%). The best fit values of the parameters A and B are written in Table 6. It is to be noted that our best fit analysis with SNe Type Ia observational 292 data also support the theoretical range of the parameters. It is also to be observed that for different α ($= 0.0020, 0.0010 \& 0.0005$) the best fit value of A and B are almost same but the value of χ_{min}^2 are different for each cases.

The 66% (solid, blue), 90% (dashed, red) and 99% (dashed, black) contours for (A, B) are plotted in figures 12, 13 and 14 for different values of α . Also the best fit values of A and B are tabulated in Table 6.

α	A	B	χ_{min}^2
0.0020	0.304936	0.266141	87260.15
0.0010	0.304936	0.266141	86928.93
0.0005	0.304936	0.266141	86863.26

Table 6: $H(z)$ - z SNe Type Ia : The best fit values of A , B and the minimum values of χ^2 for different values of α and fixed value of other parameters.

4.1. Redshift-Magnitude Observational Analysis with Supernovae Type Ia 292 Data [From Riess et al. (2004, 2007); Astier et al. (2006)]

In this subsection we measure the distance modulus (as like Sec. 3.4) of SNe Type Ia 292 data which belongs to [Riess et al. (2004, 2007); Astier et al. (2006)]. Here also we use the same luminosity distance $d_L(z)$ which is defined as

$$d_L(z) = (1+z)H_0 \int_0^z \frac{dz'}{H(z')} \quad (22)$$

and the distance modulus for SNe Type Ia observational 292 data is given below:

$$\mu(z) = 5 \log_{10} \left[\frac{d_L(z)/H_0}{1 \text{ Mpc}} \right] + 25 \quad (23)$$

As stated above, the best fit of distance modulus $\mu(z)$ which is a function of redshift z for our theoretical model and the SNe Type Ia 292 data from [Riess et al. (2004, 2007); Astier et al. (2006)] are drawn in figure 15 with most favorable different values of A , B with the previously chosen other parameters. From the curves, we can conclude that the theoretical GCCG with LQC is in agreement with the SNe Type Ia 292 data from [Riess et al. (2004, 2007); Astier et al. (2006)].

5. Study of Future Singularities

In recent time, the well established universal fact for any energy dominated model of the universe is intended to the result in future singularity. Without studying of these singularities, the ultimate goal of this study of our model become incomplete. A well known cosmological hypothesis is that the universe dominated by phantom energy ends with a future singularity, which violates the dominant energy condition (DEC), known as Big Rip[Caldwell et al. (2003)]. In 2005, Nojiri, et al. (2005) studied the various types of singularities for an phantom energy

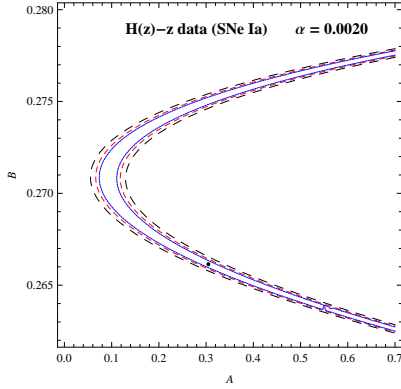


Fig.12

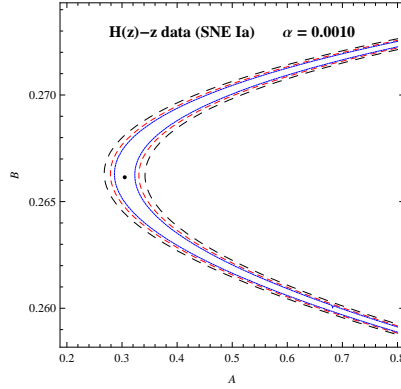


Fig.13

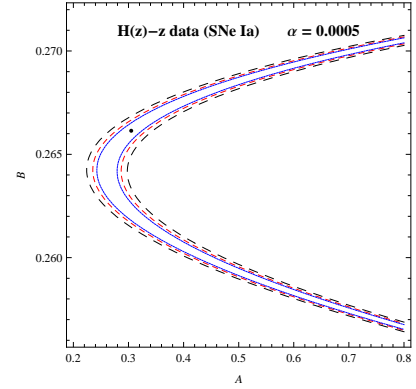


Fig.14

Fig.12-14 show that the variation of A with B for $\Omega_{m0} = 6.43 \times 10^{-8}$, $w_m = 0.051$, $\omega = -0.92$ with $\alpha = 0.0020$, 0.0010 & 0.0005 respectively for different confidence levels. The 66% (solid, blue), 90% (dashed, red) and 99% (dashed, black) contours are plotted in these figures for the $H(z)$ - z of SNe Type Ia data.

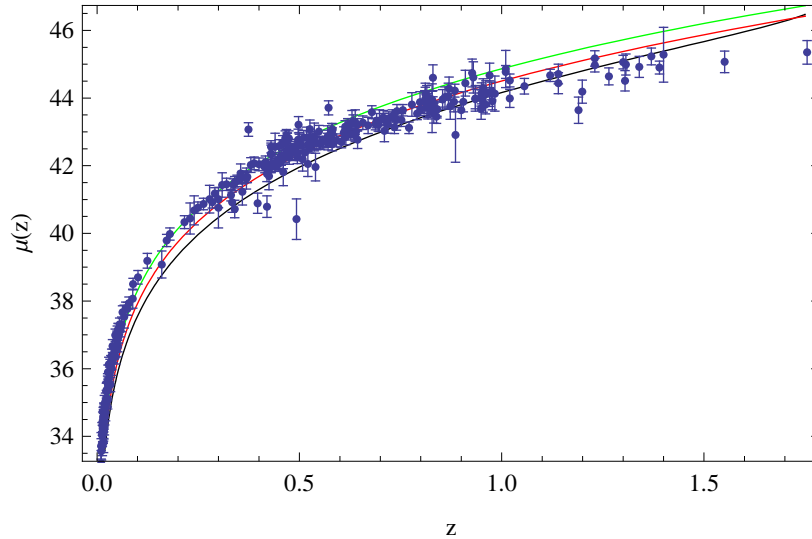


Fig.15

Fig.15 shows $\mu(z)$ vs z for our GCCG with LQC for SNe Type Ia data(dotted points) Three lines are drawn for different value of A & B ($A = 0.001$ & $B = 0.13$ for Black line; $A = 0.03$ & $B = 0.05$ for Red line; $A = 0.002$ & $B = 0.025$ for Green line).

dominated universe. There are many effective approaches have been adopted by some authors [Sami et al. (2006); Naskar et al. (2007); Samart et al. (2007); Cailleteau et al. (2008); Singh (2009); Corichi et al. (2009); Lamon et al. (2010); Singh et al. (2011)] to study the future singularities. Singularities are basically characterized by the growth of energy and curvature at the time of occurrence of them. It is observed that the quantum effects are not only very dominant near the singularities, they may prevent these singularities. All different types of future singularities for different scenario was discussed by Nojiri, et al. (2011). Recently Bamba et al. (2013) studied future singularities in the context of LQC and shown that some of these singularities may be avoided. In this regards some works have been done by Rudra et al. (2012a); Chowdhury et al. (2013); Rudra et al. (2012b). Future singularities are basically classified in four types and in each cases our model have been tested for those scenarios as follows:

- **TYPE-I Singularity (Big Rip):** When $\rho \rightarrow \infty$ and $|p| \rightarrow \infty$ for $a \rightarrow \infty$ and $t \rightarrow t_s$.

In this present scenario our predicted model of LQC with GCCG and DM in non interacting scenario have been tested and we have

$$a \rightarrow \infty : \begin{array}{ll} \rho_x \rightarrow \infty & \text{for } 1 + \omega < 0 \Rightarrow |p_x| \rightarrow 0 \\ \rho_x \rightarrow (C + 1)^{\frac{1}{\alpha+1}} & \text{for } 1 + \omega > 0 \Rightarrow |p_x| \rightarrow (C + 1)^{\frac{1}{\alpha+1}} \end{array}$$

and from the above results we can conclude that there is no possibility of Type-I i.e., “Big Rip” singularity and the result is absolutely accordance with the work of some authors [Gonzalez-Diaz (2003); Bamba et al. (2013); Chowdhury et al. (2013)] who have shown that “Big Rip” can be easily avoided in LQC with non interacting GCCG and DM and produced a singularity free late universe.

- **TYPE-II Singularity (Sudden):** When $\rho \rightarrow \rho_s$ and $|p| \rightarrow \infty$ for $a \rightarrow a_s$ and $t \rightarrow t_s$.

In this case we have been again considering our predicted model of LQC with non interacting GCCG and DM and we find that

$$a \rightarrow a_s \sim 0 : \begin{array}{ll} \rho_x \rightarrow \infty & \text{for } 1 + \omega > 0 \Rightarrow |p_x| \rightarrow 0 \\ \rho_x \rightarrow (C + 1)^{\frac{1}{\alpha+1}} & \text{for } 1 + \omega < 0 \Rightarrow |p_x| \rightarrow (C + 1)^{\frac{1}{\alpha+1}} \end{array}$$

and it can be concluded that there is no possibility of the Type-II or “Sudden” singularity for our predicted model.

- **TYPE-III Singularity (Big Freeze):** When $\rho \rightarrow \infty$ and $|p| \rightarrow \infty$ if $a \rightarrow a_s$ and $t \rightarrow t_s$.

In this present condition, it can be quite evidently concluded from our model of LQC with non interacting GCCG and DM that it does not support this Type-III or “Big Freeze” singularity. In this regards there are some works by some authors [Chowdhury et al. (2013); Rudra et al. (2012b)] in supports of this result.

- **TYPE-IV Singularity (Generalized Sudden):** For $t \rightarrow t_s$, $a \rightarrow a_s$, $\rho \rightarrow 0$ and $|p| \rightarrow 0$

In this regards we have expressed scale factor $a(t)$ in terms of energy density of GCCG as follows:

$$a = \left[\frac{B}{(\rho_x^{\alpha+1} - C)^{\omega+1} - 1} \right]^{\frac{1}{3(1+\alpha)(1+\omega)}}$$

and therefore it can be easily concluded that this type of singularity is not supported by our predicted LQC model with non interacting GCCG and DM.

6. Discussions

We have assumed the FRW universe in loop quantum cosmology (LQC) model filled with the dark matter and the Generalized Cosmic Chaplygin gas (GCCG) type dark energy. We present the Hubble parameter $H(z)$ in terms of the observable parameters Ω_{m0} and H_0 with the redshift z and the other parameters like A , B , w_m , ω and α . From Stern data set (12 points), we have obtained the best fit values of two arbitrary parameters (A, B) in table 2 by fixing other parameters $\Omega_{m0} = 0.0643$, $w_m = 0.051$, $\omega = -0.92$ and $\alpha = 0.002, 0.001, 0.0005$ by minimizing the χ^2 test. The bounds of the parameters (A, B) are obtained by 66%, 90% and 99% confidence levels in figures 1-3. Next due to joint analysis with BAO and CMB observations, we have also obtained the best fit values of the parameters (A, B) by fixing

the other parameters (same values) in tables 3 and 4 respectively. Also the bounds of the parameters (A, B) due to joint analysis with BAO and CMB observations are obtained by 66%, 90% and 99% confidence levels in figures 4-6 and figures 7-9 respectively. From tables 1-3, we see that when $\alpha = 0.002, 0.001$, the best-fit values of A and B are positive for all our observational data. But if $\alpha = 0.0005$, the best-fit value of A is negative and best-fit value of B is still positive for all our observational data. From the best fit value of distance modulus $\mu(z)$ for our theoretical GCCG model in LQC is drawn in figure 10. Fig 11 shows the same for different value of A & B ($A = 0.001$ & $B = 0.13$ for Black line; $A = 0.03$ & $B = 0.05$ for Red line; $A = 0.002$ & $B = 0.025$ for Green line). From the figure, we have concluded that our predicted theoretical GCCG model in LQC permitted the union2 sample data sets of SNe Type Ia. After that we have considered SNe Type Ia Riess 292 data from Riess et al. (2004, 2007); Astier et al. (2006) and tested our theoretical GCCG with LQC model by minimizing the χ^2 test (same as stated above) and obtained the bounds of the parameters (A, B) given in Table 6. When the other parameters are fixed at their suitable value as $\Omega_{m0} = 6.43 \times 10^{-8}$, $w_m = 0.051$, $\omega = -0.92$ with $\alpha = 0.0020, 0.0010$ & 0.0005 , we have drawn the figure 12-14 respectively and the best fitted values of $A = 0.304936$ & $B = 0.266141$ are almost same in every cases of α . Figure 15 shows the distance modulus $\mu(z)$ of our theoretical GCCG model in LQC together with Riess 292 data for different favorable values of A & B ($A = 0.001$ & $B = 0.13$ for Black line; $A = 0.03$ & $B = 0.05$ for Red line; $A = 0.002$ & $B = 0.025$ for Green line) vs redshift z and which depicted that our theoretical GCCG model in LQC suitably permitted with the Riess 292 data of SNe Type Ia. From the above results, we can finally conclude that our theoretical GCCG model in LQC is in agreement with the Supernovae Type Ia sample data. In addition, we have also investigated in details about the Future Singularities like Type-I, Type-II, Type-III and Type-IV that may be formed and or avoided in this model and it is found that our model is completely free from any types of future singularities.

Acknowledgements

The authors are thankful to IUCAA, Pune, India for warm hospitality where part of the work was carried out. The author (UD) is thankful to CSIR, Govt. of India for providing research project grant (No. 03(1206)/12/EMR-II).

REFERENCES

- Amanullah, R. et al., 2010, *Astrophys. J.*, 716, 712.
- Armendariz - Picon, C. et al., 2001, *Phys. Rev. D* , 63, 103510.
- Ashtekar, A., 2007, *Nuovo Cim. B*, 122, 135.
- Ashtekar, A. et al., 2003, *Adv. Theor. Math. Phys.*, 7, 233.
- Ashtekar, A. et al., 2004, *Class. Quantum. Grav.*, 21, R53.
- Ashtekar, A. et al., 2006, *Class. Quantum. Grav.*, 23, 391.
- Ashtekar, A. et al., 2008, *Phys. Rev. D*, 77, 024046.
- Ashtekar, A. et al., 2011, *Class. Quantum. Grav.*, 28, 213001.
- Astier, P. et al., 2006, *Astron. Astrophys.*, 447, 31.
- Bachall, N. A. et al, 1999, *Science* 284, 1481.
- Balart, L. et al., 2007, *Eur. Phys. J. C*, 51, 185.
- Bamba, K. et al., 2013, arXiv:1211.2968v2.
- Barris, B. J. et al., 2004, *Astrophys. J.*, 602, 571.
- Bennet, C. et al, 2000, *Phys. Rev. Lett.* 85, 2236.
- Bojowald, M., 2001, *Phys. Rev. Lett.*, 86, 5227.
- Bojowald, M., 2002, *Phys. Rev. Lett.*, 89, 261301.
- Bojowald, M., 2005, *liv. Rev. Rel.*, 8, 11.
- Bojowald, M., 2008, *liv. Rev. Rel.*, 11, 4.
- Bond, J. R. et al, 1997, *Mon. Not. Roy. Astron. Soc.*, 291, L33.
- Bouhmadi-Lpez, M. and Chimento, L. P., 2010, *Phys.Rev. D*, 82, 103506.

- Bridle, S. et al, 2003, *Science* 299, 1532.
- Cailleteau, T. et al., 2008, *Phys. Rev. Lett* 101, 251302.
- Caldwell, R. R., 2002, *Phys. Lett. B*, 545, 23.
- Caldwell, R. R. et al., 2003, *Phys. Rev. Lett.*, 91, 071301.
- Chakraborty, W., Chakraborty, S. and Debnath, U., 2007, *Grav. Cosmol*, 13, 293.
- Chakraborty, S., Debnath, U. and Ranjit, C., 2012, *Eur. Phys. J. C*, 72, 2101.
- Chen, S., Wang, B. and Jing, J., 2008, *Phys. Rev. D*, 78, 123503.
- Choudhury, T. R. and Padmanabhan, T., 2007, *Astron. Astrophys.*, 429, 807.
- Chowdhury, R. et al., 2013, *Int. J. Theor. Phys.*, 52,489.
- Corichi, A. et al., 2009, *Phys. Rev. D*, 80, 044024.
- Dao-Jun, L. and Xin-Zhou, L., 2005, *Chin. Phys. Lett.*, 22, 1600.
- Debnath, U., Banerjee, A. and Chakraborty, S., 2004, *Class. Quantum Grav.*, 21, 5609.
- del Campo, S., Herrera, R., Toloza, A., 2009, *Phys. Rev. D*, 79, 083507.
- Efstathiou, G. and Bond, J. R., 1999, *Mon. Not. R. Astro. Soc.* 304, 75.
- Eisenstein, D. J. et al[SDSS Collaboration], 2005, *Astrophys. J.* 633, 560.
- Farajollahi, H., Ravanpak, A., 2011, *Phys. Rev. D*, 84, 084017.
- Fu, X., Yu, H. and Wu, P., 2008, *Phys. Rev. D* 78, 063001.
- Ghose, S., Thakur, P. and Paul, B. C., 2012, *Mon. Not. R. Astron. Soc.*, 421, 20.
- González-Díaz, P. F., 2003, *Phys. Rev. D*, 68, 021303(R).
- Gorini, V., Kamenshchik, A. and Moschella, U., 2003, *Phys. Rev. D*, 67, 063509.
- Jain, B. and Taylor, A., 2003, *Phys. Rev. Lett.* 91, 141302.

- Jamil, M. and Debnath, U., 2011, *Astrophys Space Sci.*, 333, 3.
- Kamenshchik, A. et al., 2001, *Phys. Lett. B*, 511, 265.
- Komatsu, E. et al, 2011, *Astrophys. J. Suppl.*, 192, 18.
- Kowalaski et al, 2008, *Astrophys. J.*, 686, 749.
- Lamon, R. et al., 2010, *Phys. Rev. D*, 81, 024026.
- Lu, J. et al., 2008, *Phys. Lett. B*, 662, 87.
- Malquarti, M., et al., 2003, *Phys. Rev. D*, 68, 023512.
- Marcus, N., 1990, *Gen. Rel. Grav.*, 22, 873.
- Martin, J. and Yamaguchi, M., 2008, *Phys. Rev. D*, 77, 123508.
- Miller, D. et al, 1999, *Astrophys. J.* 524, L1.
- Morris, J. R., 2012, *Gen. Rel. Grav.*, 44, 437.
- Naskar, T. et al., 2007, *Phys. Rev. D*, 76, 063514.
- Nessaeris, S. and Perivolaropoulos, L., 2007, *JCAP*, 0701, 018.
- Nojiri, S. et al., 2005, *Phys. Rev. D*, 71, 063004.
- Nojiri, S. et al., 2011, *Phys. Rept.*, 505, 59.
- Padmanabhan, T., 2003, *Phys. Rept.*, 380, 235.
- Padmanabhan, T. and Choudhury, T. R., 2003, *Mon. Not. R. Astron. Soc.*, 344, 823.
- Paul, B. C., Thakur, P. and Ghose, S., 2010, *Mon. Not. Roy. Astron. Soc.*, 407, 415.
- Paul, B. C., Ghose, S. and Thakur, P., 2011, *Mon. Not. R. Astron. Soc.*, 413, 686.
- Peebles, P. J. E. and Ratra, B., 1988, *Astrophys. J. Lett.*, 325, L17.
- Perlmutter, S. J. et al, 1998, *Nature* 391, 51.

- Perlmutter, S. J. et al.[SNCP Collaboration], 1999, *Astrophys. J.*, 517, 565.
- Riess, A. G. et al.[Supernova Search Team Collaboration], 1998, *Astron. J.* 116, 1009.
- Riess, A. G. et al., 2004, *Astrophys. J.* 607, 665.
- Riess, A. G. et al., 2007, *Astrophys. J.*, 659, 98.
- Rovelli, C, 1998, *Liv. Rev. Rel.*, 1, 1.
- Rudra, P. et al., 2012, *Astrophys.Space Sci.* 339,53.
- Rudra, P. et al., 2012, *Astrophys.Space Sci.* 342,557.
- Sadjadi, H. M., 2013, *Eur. Phys. J. C*, 73, 2571.
- Sahni, V. and Starobinsky, A. A., 2000, *Int. J. Mod. Phys. D*, 9, 373.
- Samart, D. et al., 2007, *Phys. Rev. D*, 76, 043514.
- Sami, M. et al., 2006, *Phys. Rev. D*, 74, 043514.
- Sen, A., 2002, *J. High Energy Phys.* 0204, 48.
- Singh, P., 2009, *Class. Quant. Grav.*, 26, 125005.
- Singh, P. et al., 2011, *Phys. Rev. D*, 83, 064027.
- Spalinski, M., 2007, *J. Cosmol. Astropart. Phys.*, 05, 017.
- Spergel, D. N. et al, 2003, *Astrophys. J. Suppl.* 148, 175.
- Spergel, D. N. et al, 2007, *Astrophys. J. Suppl.* 170, 377.
- Stern, D. et al, 2010, *JCAP*, 1002, 008.
- Tedmark, M. et al, 2004, *Phys. Rev. D* 69, 103501.
- Thakur, P., Ghose, S. and Paul, B. C., 2009, *Mon. Not. R. Astron. Soc.*, 397, 1935.
- Tonry, J. L. et al., 2003, *Astrophys. J.*, 594, 1.

Wei, H., et al., 2005, *Class. Quantum. Grav.*, 22, 3189.

Weinberg, S., 1989, *Rev. Mod. Phys.*, 61, 1.

Wu, P. and Yu, H., 2007, *Phys. Lett. B*, 644, 16.

Wu, P. and Zhang, S. N., 2008, *JCAP*, 06, 007.

A. Appendix material

Table 5. SNe Ia 292 Data Set from Riess et al. (2004, 2007); Astier et al. (2006)

Name	z	$H(z)$	$\sigma(z)$	Type
SN90O	0.030	35.90	0.21	Gold
SN90T	0.040	36.38	0.20	Gold
SN90af	0.050	36.84	0.22	Gold
SN91ag	0.014	34.13	0.29	Gold
SN91U	0.033	35.53	0.21	Gold
SN91S	0.056	37.31	0.19	Gold
SN92al	0.014	34.12	0.29	Gold
SN92bo	0.017	34.70	0.26	Gold
SN92bc	0.018	34.96	0.25	Gold
SN92ag	0.026	35.06	0.25	Silver
SN92P	0.026	35.63	0.22	Gold
SN92bg	0.036	36.17	0.20	Gold
SN92bl	0.043	36.52	0.19	Gold
SN92bh	0.045	36.99	0.18	Gold
SN92J	0.046	36.35	0.21	Gold
SN92bk	0.058	37.13	0.19	Gold
SN92au	0.061	37.31	0.22	Gold
SN92bs	0.063	37.67	0.19	Gold
SN92ae	0.075	37.77	0.19	Gold
SN92bp	0.079	37.94	0.18	Gold
SN92br	0.088	38.07	0.28	Gold
SN92aq	0.101	38.70	0.20	Gold
SN93ae	0.018	34.29	0.25	Gold
SN93H	0.025	35.09	0.22	Gold
SN93ah	0.028	35.53	0.22	Gold
SN93ac	0.049	36.90	0.21	Silver
SN93ag	0.050	37.07	0.19	Gold
SN93O	0.052	37.16	0.18	Gold
SN93B	0.071	37.78	0.19	Gold
SN94S	0.016	34.50	0.27	Gold
SN94M	0.024	35.09	0.22	Gold
SN94Q	0.029	35.70	0.21	Gold
SN94T	0.036	36.01	0.21	Gold
SN94C	0.051	36.67	0.17	Silver
SN94B	0.089	38.50	0.17	Silver

Table 5—Continued

Name	z	$H(z)$	$\sigma(z)$	Type
SN95K	0.478	42.48	0.23	Gold
SN95ak	0.021	34.70	0.24	Silver
SN95E	0.011	32.95	0.35	Silver
SN95bd	0.015	34.07	0.28	Silver
SN95ac	0.049	36.55	0.20	Gold
SN95ar	0.465	42.81	0.22	Silver
SN95as	0.498	43.21	0.24	Silver
SN95aw	0.400	42.04	0.19	Gold
SN95ax	0.615	42.85	0.23	Gold
SN95ay	0.480	42.37	0.20	Gold
SN95az	0.450	42.13	0.21	Gold
SN95ba	0.388	42.07	0.19	Gold
SN95M	0.053	37.17	0.16	Silver
SN95ae	0.067	37.54	0.34	Silver
SN95ao	0.300	40.76	0.60	Silver
SN95ap	0.230	40.44	0.46	Silver
SN96E	0.425	41.69	0.40	Gold
SN96H	0.620	43.11	0.28	Gold
SN96I	0.570	42.80	0.25	Gold
SN96J	0.300	41.01	0.25	Gold
SN96K	0.380	42.02	0.22	Gold
SN96U	0.430	42.33	0.34	Gold
SN96Z	0.008	32.45	0.45	Silver
SN96bo	0.016	33.82	0.30	Silver
SN96bv	0.016	34.21	0.27	Silver
SN96bk	0.007	32.09	0.53	Silver
SN96C	0.027	35.90	0.21	Gold
SN96bl	0.034	36.19	0.20	Gold
SN96ab	0.124	39.19	0.22	Gold
SN96cf	0.570	42.77	0.19	Silver
SN96cg	0.490	42.58	0.19	Silver
SN96ci	0.495	42.25	0.19	Gold
SN96cl	0.828	43.96	0.46	Gold
SN96cm	0.450	42.58	0.19	Silver
SN96cn	0.430	42.56	0.18	Silver

Table 5—Continued

Name	z	$H(z)$	$\sigma(z)$	Type
SN96V	0.024	35.33	0.26	Silver
SN96T	0.240	40.68	0.43	Silver
SN96R	0.160	39.08	0.40	Silver
SN97eq	0.538	42.66	0.18	Gold
SN97ek	0.860	44.03	0.30	Gold
SN97ez	0.778	43.81	0.35	Gold
SN97as	0.508	42.19	0.35	Gold
SN97aw	0.440	42.56	0.40	Silver
SN97bb	0.518	42.83	0.31	Gold
SN97bh	0.420	41.76	0.23	Silver
SN97bj	0.334	40.92	0.30	Gold
SN97ce	0.440	42.07	0.19	Gold
SN97cj	0.500	42.73	0.20	Gold
SN97do	0.010	33.72	0.39	Gold
SN97E	0.013	34.02	0.31	Gold
SN97Y	0.016	34.53	0.27	Gold
SN97cn	0.017	34.71	0.28	Gold
SN97dg	0.029	36.13	0.21	Gold
SN97F	0.580	43.04	0.21	Gold
SN97H	0.526	42.56	0.18	Gold
SN97I	0.172	39.79	0.18	Gold
SN97N	0.180	39.98	0.18	Gold
SN97O	0.374	43.07	0.20	Silver
SN97P	0.472	42.46	0.19	Gold
SN97Q	0.430	41.99	0.18	Gold
SN97R	0.657	43.27	0.20	Gold
SN97ac	0.320	41.45	0.18	Gold
SN97af	0.579	42.86	0.19	Gold
SN97ai	0.450	42.10	0.23	Gold
SN97aj	0.581	42.63	0.19	Gold
SN97am	0.416	42.10	0.19	Gold
SN97ap	0.830	43.85	0.19	Gold
SN97ck	0.970	44.13	0.38	Silver
SN98ax	0.497	42.77	0.31	Silver
SN98aw	0.440	42.02	0.19	Silver

Table 5—Continued

Name	z	$H(z)$	$\sigma(z)$	Type
SN98ay	0.638	43.29	0.36	Silver
SN98ba	0.430	42.36	0.25	Gold
SN98be	0.644	42.77	0.26	Silver
SN98as	0.355	41.77	0.28	Silver
SN98bi	0.740	43.35	0.30	Gold
SN98ac	0.460	41.81	0.40	Gold
SN98M	0.630	43.26	0.37	Gold
SN98J	0.828	43.59	0.61	Gold
SN98I	0.886	42.91	0.81	Silver
SN98bp	0.010	33.20	0.38	Gold
SN98ef	0.017	34.18	0.26	Gold
SN98V	0.017	34.47	0.26	Gold
SN98co	0.017	34.62	0.27	Gold
SN98eg	0.023	35.35	0.22	Gold
SN98cs	0.032	36.08	0.20	Gold
SN98dx	0.053	36.95	0.19	Gold
SN99Q2	0.459	42.67	0.22	Gold
SN99U2	0.511	42.83	0.21	Gold
SN99S	0.474	42.81	0.22	Gold
SN99N	0.537	42.85	0.41	Gold
SN99M	0.493	40.42	0.60	Silver
SN99fn	0.477	42.38	0.21	Gold
SN99ff	0.455	42.29	0.28	Gold
SN99fj	0.815	43.75	0.33	Gold
SN99fm	0.949	44.00	0.24	Gold
SN99fk	1.056	44.35	0.23	Gold
SN99fw	0.278	41.01	0.41	Gold
SN99cp	0.010	33.56	0.37	Gold
SN99dq	0.013	33.73	0.30	Gold
SN99dk	0.014	34.43	0.29	Gold
SN99aa	0.015	34.58	0.28	Gold
SN99X	0.025	35.40	0.22	Gold
SN99gp	0.026	35.57	0.21	Gold
SN99cc	0.031	35.84	0.21	Gold
SN99ef	0.038	36.67	0.19	Gold

Table 5—Continued

Name	z	$H(z)$	$\sigma(z)$	Type
SN99fv	1.199	44.19	0.34	Gold
SN99fh	0.369	41.62	0.31	Silver
SN99da	0.012	34.05	0.36	Silver
SN00ec	0.470	42.76	0.21	Gold
SN00dz	0.500	42.74	0.24	Gold
SN00ea	0.420	40.79	0.32	Silver
SN00eg	0.540	41.96	0.41	Gold
SN00ee	0.470	42.73	0.23	Gold
SN00eh	0.490	42.40	0.25	Gold
SN00fr	0.543	42.67	0.19	Gold
SN00dk	0.016	34.41	0.27	Gold
SN00B	0.019	34.59	0.25	Gold
SN00fa	0.021	35.05	0.23	Gold
SN00cn	0.023	35.14	0.22	Gold
SN00bk	0.026	35.35	0.23	Gold
SN00cf	0.036	36.39	0.19	Gold
SN00ce	0.016	34.47	0.26	Silver
SN01iv	0.397	40.89	0.30	Silver
SN01iw	0.340	40.72	0.26	Silver
SN01jh	0.884	44.22	0.19	Gold
SN01hu	0.882	43.89	0.30	Gold
SN01ix	0.710	43.03	0.32	Silver
SN01iy	0.570	42.87	0.31	Gold
SN01jp	0.528	42.76	0.25	Gold
SN01V	0.016	34.13	0.27	Gold
SN01fo	0.771	43.12	0.17	Gold
SN01fs	0.873	43.75	0.38	Silver
SN01hs	0.832	43.55	0.29	Gold
SN01hx	0.798	43.88	0.31	Gold
SN01hy	0.811	43.97	0.35	Gold
SN01jb	0.698	43.33	0.32	Silver
SN01jf	0.815	44.09	0.28	Gold
SN01jm	0.977	43.91	0.26	Gold
SN01kd	0.935	43.99	0.38	Silver
SN02P	0.719	43.22	0.26	Silver

Table 5—Continued

Name	z	$H(z)$	$\sigma(z)$	Type
SN02ab	0.422	42.02	0.17	Silver
SN02ad	0.514	42.39	0.27	Silver
1997ff	1.755	45.35	0.35	Gold
2002dc	0.475	42.24	0.20	Gold
2002dd	0.950	43.98	0.34	Gold
2003aj	1.307	44.99	0.31	Silver
2002fx	1.400	45.28	0.81	Silver
2003eq	0.840	43.67	0.21	Gold
2003es	0.954	44.30	0.27	Gold
2003az	1.265	44.64	0.25	Silver
2002kc	0.216	40.33	0.19	Silver
2003eb	0.900	43.64	0.25	Gold
2003XX	0.935	43.97	0.29	Gold
2002hr	0.526	43.08	0.27	Silver
2003bd	0.670	43.19	0.24	Gold
2002kd	0.735	43.14	0.19	Gold
2003be	0.640	43.01	0.25	Gold
2003dy	1.340	44.92	0.31	Gold
2002ki	1.140	44.71	0.29	Gold
2003ak	1.551	45.07	0.32	Silver
2002hp	1.305	44.51	0.30	Gold
2002fw	1.300	45.06	0.20	Gold
HST04Pat	0.970	44.67	0.36	Gold
HST04Mcg	1.370	45.23	0.25	Gold
HST05Fer	1.020	43.99	0.27	Gold
HST05Koe	1.230	45.17	0.23	Gold
HST05Dic	0.638	42.89	0.18	Silver
HST04Gre	1.140	44.44	0.31	Gold
HST04Omb	0.975	44.21	0.26	Gold
HST05Red	1.190	43.64	0.39	Silver
HST05Lan	1.230	44.97	0.20	Gold
HST04Tha	0.954	43.85	0.27	Gold
HST04Rak	0.740	43.38	0.22	Gold
HST05Zwi	0.521	42.05	0.37	Silver
HST04Hawk	0.490	42.54	0.24	Silver

Table 5—Continued

Name	z	$H(z)$	$\sigma(z)$	Type
HST04Kur	0.359	41.23	0.39	Silver
HST04Yow	0.460	42.23	0.32	Gold
HST04Man	0.854	43.96	0.29	Gold
HST05Spo	0.839	43.45	0.20	Gold
HST04Eag	1.020	44.52	0.19	Gold
HST05Gab	1.120	44.67	0.18	Gold
HST05Str	1.010	44.77	0.19	Gold
HST04Sas	1.390	44.90	0.19	Gold
SN88U	0.309	41.43	0.36	Silver
SN-03D1au	0.504	42.61	0.17	Gold
SN-03D1aw	0.582	43.07	0.17	Gold
SN-03D1ax	0.496	42.36	0.17	Gold
SN-03D1bp	0.346	41.55	0.17	Silver
SN-03D1cm	0.870	44.28	0.34	Gold
SN-03D1co	0.679	43.58	0.19	Gold
SN-03D1ew	0.868	44.06	0.38	Silver
SN-03D1fc	0.331	41.13	0.17	Gold
SN-03D1fl	0.688	43.23	0.17	Gold
SN-03D1fq	0.800	43.67	0.19	Gold
SN-03D1gt	0.548	43.01	0.18	Silver
SN-03D3af	0.532	42.78	0.18	Gold
SN-03D3aw	0.449	42.05	0.17	Gold
SN-03D3ay	0.371	41.67	0.17	Gold
SN-03D3ba	0.291	41.18	0.17	Silver
SN-03D3bh	0.249	40.76	0.17	Gold
SN-03D3cc	0.463	42.27	0.17	Gold
SN-03D3cd	0.461	42.22	0.17	Gold
SN-03D4ag	0.285	40.92	0.17	Gold
SN-03D4at	0.633	43.32	0.18	Gold
SN-03D4aud	0.468	42.89	0.18	Silver
SN-03D4bcd	0.572	43.71	0.21	Silver
SN-03D4cn	0.818	43.72	0.34	Silver
SN-03D4cx	0.949	43.69	0.32	Gold
SN-03D4cy	0.927	44.74	0.41	Silver
SN-03D4cz	0.695	43.21	0.19	Gold

Table 5—Continued

Name	z	$H(z)$	$\sigma(z)$	Type
SN-03D4dh	0.627	42.93	0.17	Gold
SN-03D4di	0.905	43.89	0.30	Gold
SN-03D4dy	0.604	42.70	0.17	Gold
SN-03D4fd	0.791	43.54	0.18	Gold
SN-03D4gf	0.581	42.95	0.17	Silver
SN-03D4gg	0.592	42.75	0.19	Gold
SN-03D4gl	0.571	42.65	0.18	Gold
SN-04D1ag	0.557	42.70	0.17	Gold
SN-04D1aj	0.721	43.39	0.20	Silver
SN-04D1ak	0.526	42.83	0.17	Silver
SN-04D2cf	0.369	41.67	0.17	Gold
SN-04D2fp	0.415	41.96	0.17	Gold
SN-04D2fs	0.357	41.63	0.17	Gold
SN-04D2gb	0.430	41.96	0.17	Gold
SN-04D2gc	0.521	42.62	0.17	Silver
SN-04D2gp	0.707	43.42	0.21	Gold
SN-04D2iu	0.691	43.33	0.21	Silver
SN-04D2ja	0.741	43.61	0.20	Silver
SN-04D3co	0.620	43.21	0.18	Gold
SN-04D3cp	0.830	44.60	0.38	Silver
SN-04D3cy	0.643	43.21	0.18	Gold
SN-04D3dd	1.010	44.86	0.55	Silver
SN-04D3df	0.470	42.45	0.17	Gold
SN-04D3do	0.610	42.98	0.17	Gold
SN-04D3ez	0.263	40.87	0.17	Gold
SN-04D3fk	0.358	41.66	0.17	Gold
SN-04D3fq	0.730	43.47	0.18	Gold
SN-04D3gt	0.451	42.22	0.17	Silver
SN-04D3gx	0.910	44.44	0.38	Silver
SN-04D3hn	0.552	42.65	0.17	Gold
SN-04D3is	0.710	43.36	0.18	Silver
SN-04D3ki	0.930	44.61	0.46	Silver
SN-04D3kr	0.337	41.44	0.17	Gold
SN-04D3ks	0.752	43.35	0.19	Silver
SN-04D3lp	0.983	44.13	0.52	Silver

Table 5—Continued

Name	z	$H(z)$	$\sigma(z)$	Type
SN-04D3lu	0.822	43.73	0.27	Gold
SN-04D3ml	0.950	44.14	0.31	Gold
SN-04D3nc	0.817	43.84	0.30	Silver
SN-04D3nh	0.340	41.51	0.17	Gold
SN-04D3nr	0.960	43.81	0.28	Silver
SN-04D3ny	0.810	43.88	0.34	Silver
SN-04D3oe	0.756	43.64	0.17	Gold
SN-04D4an	0.613	43.15	0.18	Gold
SN-04D4bk	0.840	43.66	0.25	Silver
SN-04D4bq	0.550	42.67	0.17	Gold
SN-04D4dm	0.811	44.13	0.31	Gold
SN-04D4dw	0.961	44.18	0.33	Gold